Preprints, Seventh Conference on Polar Meteorology and Oceanography and Joint Symposium on High-Latitude Climate Variations, Hyannis, Mass., 12-16 May, 2003

3.21 PACK ICE SURFACE ENERGY CHANGES AT SHEBA INITIATED BY LATE SUMMER SYNOPTIC FORCING

P. Ola G. Persson[1], Edgar L Andreas[2], Christopher W. Fairall[3], Peter S. Guest[4], and Donald K. Perovich[2]

[1]Cooperative Institute for Research in Environmental Sciences/NOAA/ETL, Boulder, Colorado
[2]U.S. Army Cold Regions Research and Engineering Laboratory, Hanover, New Hampshire
[3]NOAA Environmental Technology Laboratory, Boulder, Colorado
[4]Naval Postgraduate School, Monterey, California

1. INTRODUCTION

Seasonal changes in the Arctic may consist of a series of episodic transitions triggered by one or, at most, a few major atmospheric synoptic events, and hence occurring on a time scale of a few days. Indeed, Ruffieux, et al. (1995) inferred from their springtime energy budget measurements over the pack ice in the Beaufort Sea that "the seasonal transition to summertime conditions may occur with very strong synoptic events, rather than through gradual heating processes." In their case, the synoptic event produced changes in numerous surface energy budget terms, the surface temperature, and the number and areal coverage of open leads. Hence, an understanding of the impacts of major synoptic events on the Arctic pack ice environment is necessary to understand the Arctic climate and seasonal changes. This impact may extend beyond the atmosphere or surface energy budget terms to include effects in the ice and ocean as well.

In this paper, we use the extensive suite of measurements from the Surface Heat Budget of the Arctic Ocean (SHEBA) ice camp (Perovich et al. 1999; Uttal et al. 2002) to examine such a major transition event that occurred in late summer. It was the first, and arguably largest, step in the transition from a summer melt regime to freeze-up, which occurred later in August. The SHEBA data are used to characterize the atmospheric, ice, and oceanic structure just prior to, during, and just after this event, and to show how the synoptically produced changes in the atmosphere led to changes through the entire SHEBA column. The general description of the data sets are provided by Perovich et al. (1999) and Uttal et al. (2002), while more detailed descriptions are given by Persson et al (2002) for the Atmospheric Surface Flux Group (ASFG) data and Perovich et al (2002a, 2002b) for the ice and snow measurements made by the Ice Physics Group (IPG).

Corresponding author: Dr. Ola Persson, CIRES/NOAA/ETL, R/ET7, 325 Broadway, Boulder, CO 80305. e-mail:ola.persson@noaa.gov

2. ATMOSPHERIC SYNOPTIC EVOLUTION

In July and August 1998, the SHEBA camp was located on the pack ice in the Chukchi Sea near 78°N, 161-166°W. During these two months, three main synoptic events occurred (Fig. 1), producing significant reduction in surface pressure. Though the first event (July 4-5) was well organized and brought significant rainfall to the ice camp, the baroclinicity (temperature change) associated with this event was modest and was limited in altitude primarily to the lower and middle levels (1-6 km) of the troposphere. This was not a significant transitional event. Note that the top of the Arctic inversion near 1 km was above freezing for the entire period from before July 1 to July 29, with temperatures above 8°C at an altitude of 300-1500 m for the period July 18-26 (JD 199-207).

In contrast, event E2 showed large temperature changes throughout the troposphere, and even into the lower stratosphere. This event actually consisted of three cold frontal passages (vertical dashed lines in Fig. 1; see also Figs. 2 and 3) during a period of 5 days (July 27-Aug. 1; JD208-213). Each frontal passage produced a step change in temperature, with the total cooling from the three frontal passages during this event being about 10-15°C above the lowest 300 m. Near the surface, the air temperature cooled only about 2°C because of the modifying effect of the pack ice. Note also that the tropopause descended nearly 2 km during this event. During these days, the SHEBA ice camp went from being influenced by warm, southerly, low-level winds from Siberia to much colder westerly or northwesterly winds at all levels that had an appearance of a circumpolar vortex (e.g., Fig. 2d). Hence, the post-event air at all levels had much longer trajectories over the pack ice. Both events E1 and E2 produced significant precipitation. In the case of E2, the precipitation began as rain but

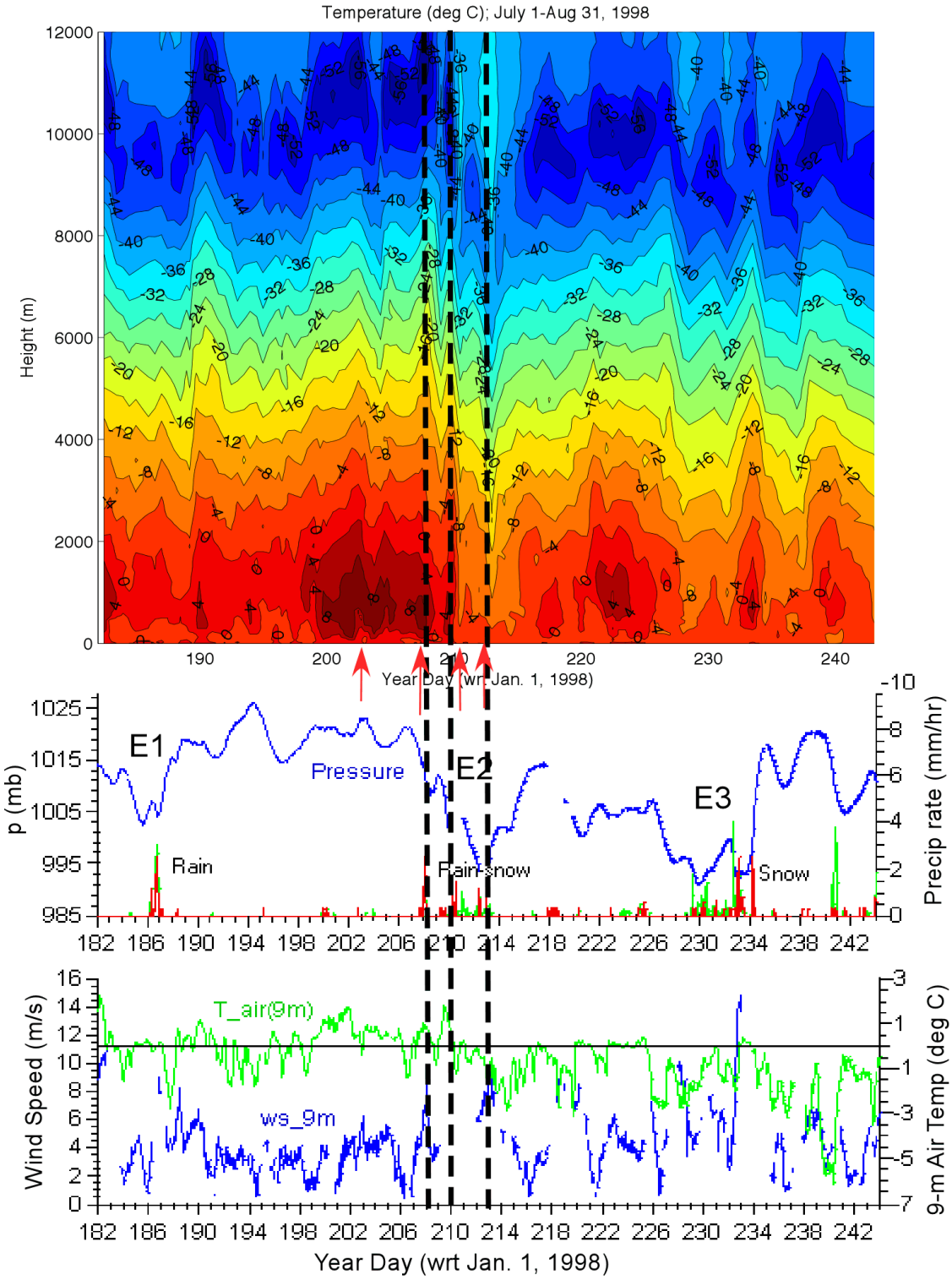

Fig. 1: Meteorological evolution at the SHEBA ice camp during July and August, 1998. Shown are a) time-height series of temperature from the rawinsondes and the ASFG tower data, b) surface pressure (blue) and precipitation rate (green - optical raingauge and red - tipping bucket), and c) 9-m air temperature (green) and wind speed (blue) from the ASFG tower. Times for the three synoptic events (E1, E2, and E3), the three cold-frontal passages associated with event E2 (dashed vertical lines), and the satellite images in Fig. 2 (red arrows) are all shown.

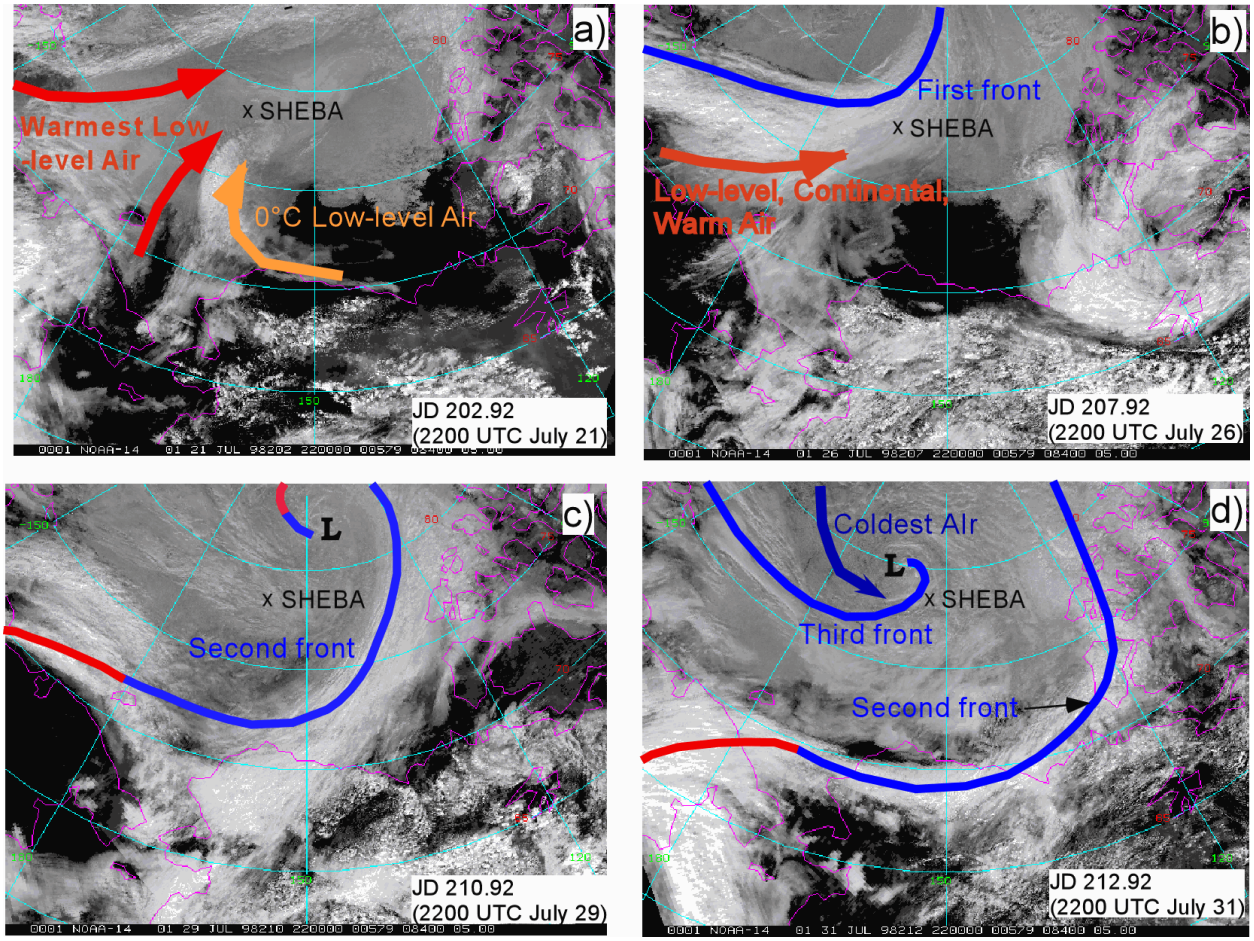

Fig. 2: Visible satellite images at 22 UTC on a) July 21, b) July 26, c) July 29, and d) July 31 showing the low-level airflows (color-coded arrows with red being warmest and blue coldest) and cold (blue) and warm (red) fronts. The outlines of the land are shown in purple, and the SHEBA site is marked by "X".

changed to ice pellets with the second front and then finally to snow near 12 UTC on July 29 (JD210.5) (Fig. 3).

Event E3 was also a multi-frontal event extending over a six-day period (Aug. 15-21; JD227-233). Arguably, it could be divided into two events. Like event E2, it showed baroclinicity through the depth of the troposphere and into the lower stratosphere, though these changes were only about 60-80% of those noted for E2. Again, changes of near-surface temperature were the most subtle compared to other levels in the atmospheric column. With event E3, the near-surface air temperatures became consistently below freezing, and the summer surface melt season came to an end. Both events E2 and E3 are seasonally and climatologically important transitional synoptic events. Because it was slightly stronger and caused significant changes throughout the SHEBA column, event E2 is the focus of this paper.

All three synoptic events were accompanied by significant increases in wind speed, with the last two events having near-surface wind speeds over 10 ms^{-1} (Fig. 1c) and the accompanying large increases in surface stress (not shown).

3. SURFACE ENERGY BUDGET

3.1 Surface energy budget definitions

We will now consider a surface slab of finite thickness consisting of ice with melt ponds, similar to that near the ASFG measurement site. The total energy flux, F_{tot}, from the atmosphere into this surface slab is given by

$$F_{tot} = Q^* - H_s - H_l + C, \qquad (3.1)$$

where Q^* is the total net radiative flux given by

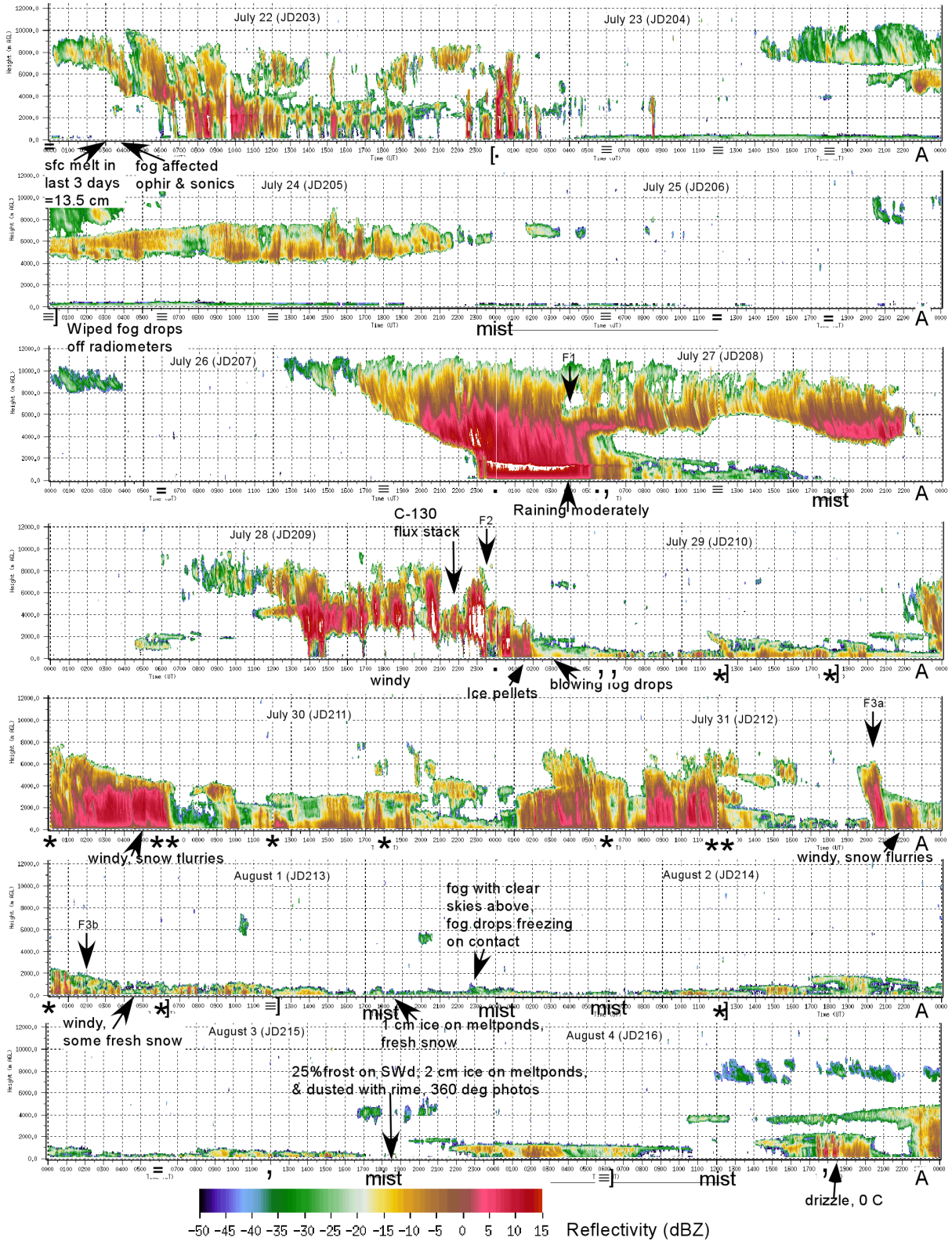

Fig. 3: Cloud radar time-height sections from 0-12 km at the SHEBA site from July 22- Aug. 4, 1997. ASFG logbook annotations are indicated on the time axis, as are the ship's bridge 6-hourly weather observations. The three frontal passages with event E2 are marked as F1, F2 and F3.

$$Q^* = Q_s + Q_l$$
$$= Q_{si} - Q_{so} + Q_{li} - Q_{lo}$$
$$= Q_{si}(1-\alpha) + Q_l , \quad (3.2)$$

H_s is the turbulent sensible heat flux, H_l is the turbulent latent heat flux, Q_s and Q_l are net shortwave and longwave radiative fluxes, and C is the conductive flux through the ice. The subscripts "i" and "o" indicate the incoming and outgoing radiative fluxes, respectively, and α is the surface albedo.

Note that (3.2) assumes that all radiative flux is absorbed within this surface slab, implying a slab thickness of 1-2 m for ice. Even with this ice thickness, a monthly average of 1-7 Wm^{-2} of solar energy penetrates through the ice into the ocean during July and August (using an ice extinction coefficient of 1.5 m^{-1} [*Maykut and Untersteiner*, 1971]), so (3.2) slightly overestimates the energy input from above to this surface slab during these months.

During July and August when there is generally no snow cover, the conductive flux is calculated from the measured surface temperature (T_s) using the water temperature at the bottom of the ice (T_w = -1.8° C), the approximate ice thickness (d_i = 2.0 m), the thermal conductivity of the ice (k_i = 2.0 W m^{-1} K^{-1}), and

$$C = -k_i [(T_s - T_w)/d_i]. \quad (3.3)$$

All terms on the right-hand side of (3.1) and (3.2) are directly measured at the ASFG site except C, which is calculated from (3.3). To increase the number of data points, the median value of H_s from the five levels for each hour is used. Though H_l was directly measured through covariance techniques, its bulk estimate at 10 m, H_{lb}, is used in the calculations presented here. Using H_{lb} rather than H_l reduces the latent heat flux slightly during August and improves the data recovery. The energy budget was calculated at hourly intervals.

The total energy flux at a given time may be positive, negative, or zero. If F_{tot} is positive, the ice is gaining energy, which can be used to either increase the temperature of the ice (energy storage) or, if the temperature is already at the melting point, to produce melting. If F_{tot} is negative, energy is lost by the surface slab, and the surface water freezes or the slab temperature decreases. Note that we are including only the change of phase in this surface slab, not the change of phase at the bottom of the ice.

3.2 Surface energy budget changes

The time series of the total energy flux (F_{tot}) indicates two times of transition when the 24-hour running mean of F_{tot} decreases near event E2 (Fig. 4b). The first decrease of about 31 Wm^{-2} occurs as the warm air at 500 m associated with the first cold front reaches the SHEBA site, about 24 hours before the passage of the first front at 04 UTC July 27 (JD208). That the transition occurs about 24 hours earlier than we might have expected appears attributable to the fortuitous timing of the nighttime clear skies leading to surface freezing and an increased albedo, followed by thickening clouds the next morning at the time the Q_{si} would be increasing (see Fig. 3). The second decrease of about 27 Wm^{-2} occurs near 12 UTC on JD212, near the passage of the third front. Note that no obvious transition in F_{tot} occurs with the second front near 00 UTC July 29 (JD210). Hence, frontal passages don't necessarily produce transitions in F_{tot}.

We will now examine the terms of the surface energy budget more carefully to determine the physical processes leading to this decrease in F_{tot} from 90 Wm^{-2} to 32 Wm^{-2} associated with event E2. Since we are interested in the contribution of changes of individual terms to the changes of F_{tot}, we use (3.1) and (3.2) to obtain the change in F_{tot} at a transition between two arbitrary time periods

$$\Delta F_{tot} = F_{tot2} - F_{tot1}$$
$$= \Delta Q^* - \Delta H_s - \Delta H_l + \Delta C, \quad (3.4)$$

where

$$\Delta Q^* = \Delta Q_s + \Delta Q_l \quad (3.5a)$$
$$= \Delta Q_{si} - \Delta Q_{so} + \Delta Q_{li} + \Delta Q_{lo} \quad (3.5b)$$
$$= (1-\alpha_1)\Delta Q_{si} + \Delta Q_{li} - \Delta Q_{lo} - Q_{si2}\Delta\alpha . \quad (3.5c)$$

The subscripted numbers indicate values for either period 1 or 2, and Δ indicates the difference of period 2 minus period 1. Because the albedo changes during this event, (3.5c) was formulated to explicitly include the effect of the change of albedo on F_{tot}, given by the last term in (3.5c).

Figure 4 shows that the albedo at the ASFG radiometer increased from an average of 0.50 in period P1 to 0.61 in P2 and to 0.66 in P3. The IPG albedo measurements, made along a 200-m long line every other day near solar noon, also showed an increase, with the average albedo over the pack ice points (excluding meltponds and leads) increasing about 0.04 during the first transition and 0.06 during the second. The lower

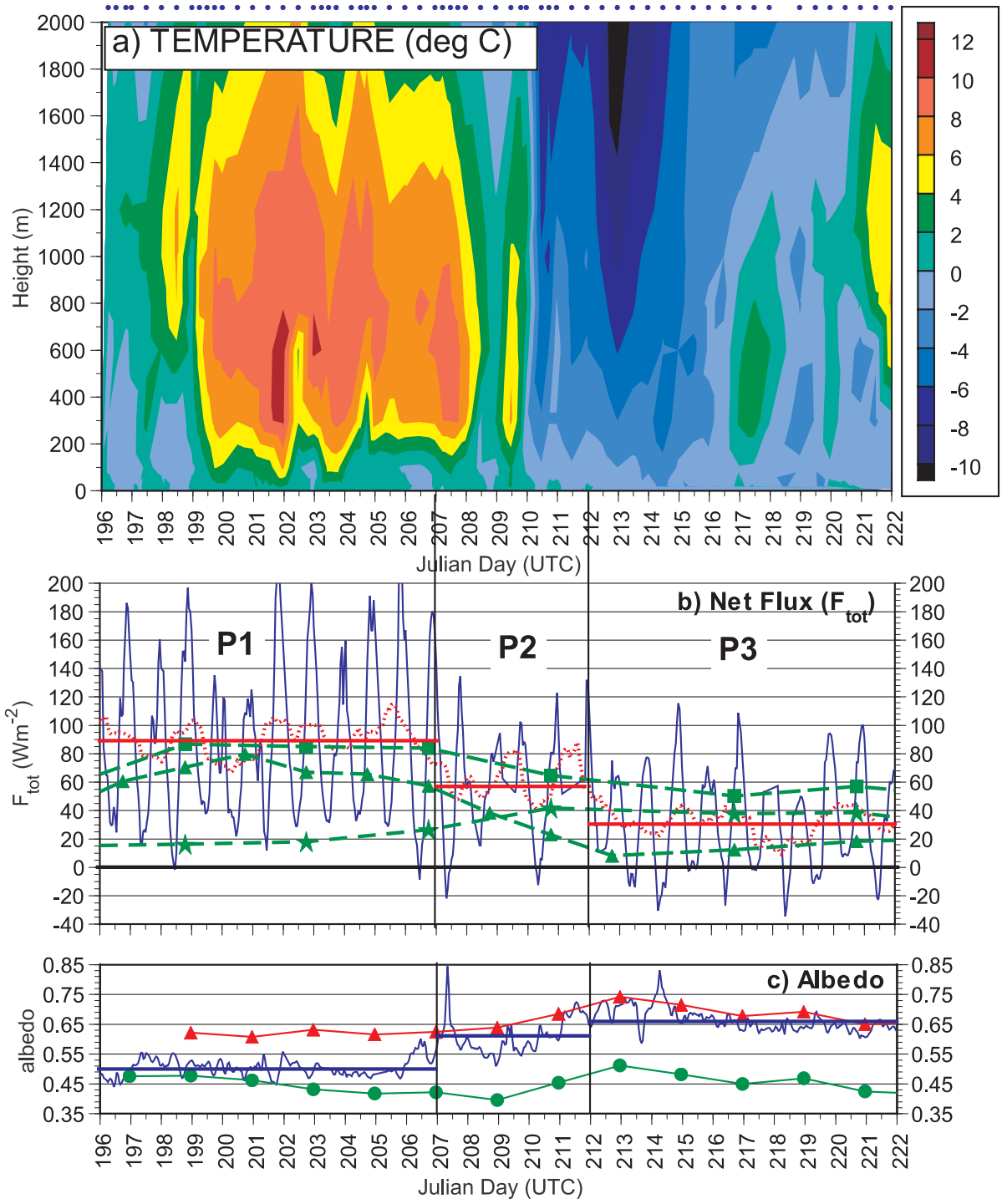

Fig. 4: a) Time-height series of temperatures in the lowest 2 km from soundings at times indicated by the blue dots at the top, b) hourly (blue), 24-hour running mean (red dotted), and period means (red solid) of F_{tot}, and c) the hourly albedo from the ASFG radiometer site (thin blue), the mean albedo from the ASFG site (heavy blue line), the mean bare ice albedo (red triangles) along the 200-m IPG albedo line taken near solar noon every other day, and the mean albedo along the IPG line (green dots). The vertical black lines show times of apparent transition for F_{tot} dividing the data into time periods P1, P2, and P3. In b), the green points show the heat fluxes implied by the surface (triangle), bottom (star), and total (square) ice melt given in Fig. 6.

ASFG ice albedos during P1 are probably due to the meltpond that was within the viewing area of the ASFG radiometer. During P2 and P3, the ASFG albedo is in excellent agreement with the average IPG ice albedo, as the meltpond near the ASFG radiometer acquired a thin ice surface (see Fig. 2d of Persson et al 2002). An interesting sidelight is that several peaks in albedo correspond to nighttime negative F_{tot} values (Figs. 4b and 4c), implying some surface freezing. Note the large increase in the occurrence of these nighttime negative F_{tot} values from before to after event E2. A dusting of snow both ahead of and behind the last front also contributed to the albedo increase (see Fig. 1b and Fig. 3).

We will also make use of the definition of sky temperature

$$T_{sky} = (Q_{li}/\varepsilon_{sky})^{0.25}, \qquad (3.6)$$

where we are assuming that the sky behaves as a black body with $\varepsilon_{sky} = 1.0$.

Figure 5 shows the 24-hour running mean time series of the crucial surface energy parameters, and Table 1 gives the mean values of all of the surface energy terms for the periods P1, P2, and P3 and the magnitudes of their changes across the transitions. The largest change occurs for Q_{si} as it decreases by about 42 Wm^{-2} from period 1 to period 2 (Fig. 5a), presumably because of greater attenuation by clouds. This occurs by either a change in cloud microphysics (an increase in the optical thickness of the clouds) or by an increase of the cloud fraction. Inspection of the cloud radar

Table 1. Mean values of the surface energy budget terms for each of the three time periods P1, P2, and P3. The change in each term at transitions 1 and 2 are in the columns headed with $\Delta 1$ and $\Delta 2$, respectively. The row labeled "sum" is the sum of the terms labeled with letters.

	JD 196-207 (P1)	**Δ1**	**JD 207-212 (P2)**	**Δ2**	**JD 212-222 (P3)**
F_{tot}	89.8	-31.0	58.9	-27.0	31.9
Sum (a+b+c+d+e)		-33.7		-22.0	
Q_{si}	198.5	-42.0	156.5	5.7	162.2
Q_{so}	99.3	5.6	93.7	-13.6	107.3
Q_{li}	305.8	-6.3	299.5	-3.3	296.2
Q_{lo}	315.4	0.7	314.7	2.6	312.1
Q_s	99.1	-36.3	62.8	-8.0	54.9
Q_l	-9.6	-5.6	-15.2	-0.6	-15.8
Q*	89.5	-41.9	47.6	-8.6	39.0
a) $(1-\alpha_1)*Q_{si}+Q_l$	89.6	-26.6	63.0		
a) $(1-\alpha_2)*Q_{si}+Q_l$			45.8	1.6	47.4
b) $Q_{si}*(\alpha-\alpha_1)$	-1.5	-15.3	-16.8		
b) $Q_{si}*(\alpha-\alpha_2)$			0.3	-9.9	-9.6
c) H_s	-2.0	8.4	-10.4	-12.6	2.2
d) H_{lb}	0.3	-0.3	0.6	-1.6	2.2
e) C	-1.8	0.1	-1.6	0.6	-1.1
α	0.50		0.61		0.66

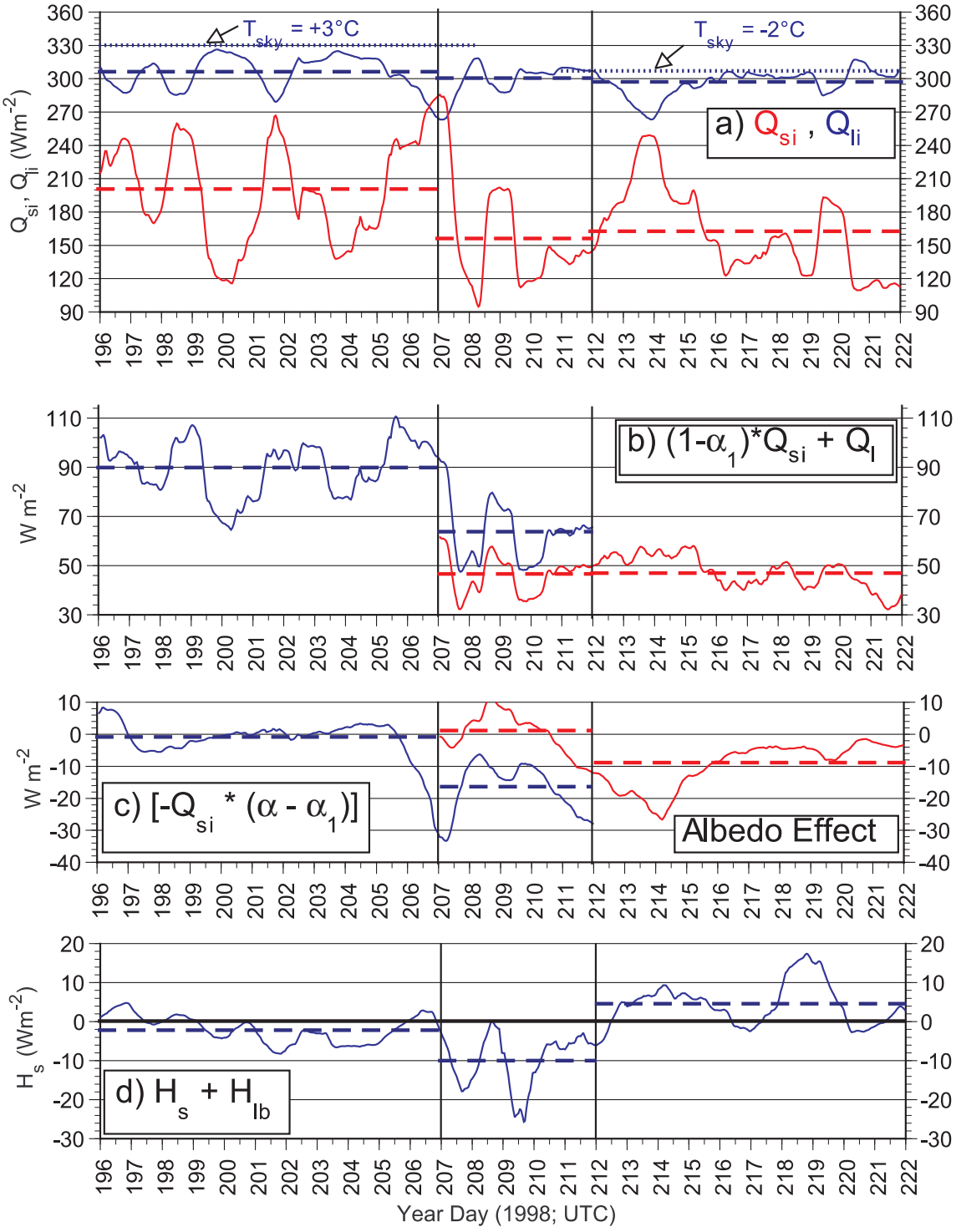

Fig. 5: Time series of a) incoming shortwave (Q_{si}) and longwave (Q_{li}) radiation, b) directly absorbed radiation normalized to α_1, c) the albedo effect (see text), and d) the turbulent heat flux (H_s + H_{lb}). A 24-hour running mean filter has been applied to all of the data. Two transition periods (vertical black lines) are shown, and the mean value of each quantity for each time period is given by the dashed lines. In a), the Q_{li} giving blackbody sky temperatures (T_{sky}) of the given values are shown as dotted lines. In b) and c), the reference albedo α_1 is that for period 1 (blue) and period 2 (red).

backscatter (Fig. 3) does not provide an obvious answer, though deeper clouds with presumably a large optical thickness do occur preferentially in period 2. Further diagnosis of the cloud radar and cloud lidar data (Intrieri et al. 2002) are needed to determine the reason for this decrease in Q_{si} from period 1 to period 2. A slight increase in Q_{si} occurs from period 2 to period 3 in Fig. 5. Note that (3.5c) shows that only about half of the change in incoming solar radiation is realized as a change in F_{tot} because of the effect of the albedo.

Even though Q_{si} and Q_{li} are anticorrelated in any one period due to the effect of clouds (with the cloud effect on Q_{si} being larger than the effect on Q_{li}), a decrease in Q_{li} of 6.3 W m^{-2} occurs along with the decrease in Q_{si} at the transition from periods 1 to 2. An additional decrease in Q_{li} of 3.3 W m^{-2} occurs between periods 2 and 3. Note that Q_{li} for cloudy periods decreases about 23 Wm^{-2} from period 1 to periods 2 and 3 because the effective radiative temperature of the clouds has decreased from +3°C to -2°C. Hence, with the surface temperature fixed at 0°C, clouds during period 1 would produce a positive net longwave flux, while Q_l would be negative for cloudy times during period 2. Because the surface temperature changes very little across either of these transitions (Fig. 1c), Q_{lo} decreases only by 3.3 Wm^{-2} from period 1 to period 3, producing a net decrease of Q_l of 6.3 Wm^{-2}. Hence, the large decrease in Q_{si} at the first transition may have been due to an increase in optical thickness, and the unusual accompanying decrease in Q_{li} has come about through the cooling of the air mass aloft, through a change in height of the cloud base, or, most likely, through both. Again, the data from the cloud radar and lidar need to be studied to determine if the character of the clouds have changed, especially at transition 1.

The direct effect of the change of incoming radiation on F_{tot} is understood by examining the time series of the first two terms of (3.5c). Figure 5b shows that a decrease of 26.6 W m^{-2} occurs at the first transition, while the change is negligible at the second. Recall that 9.6 W m^{-2} of this was due to changes in Q_{li}, so the remainder (17 Wm^{-2}) is due to the decrease in Q_{si}. The effect of the change in albedo contributes a decrease of 15.3 W m^{-2} at transition 1 and an additional decrease of 9.9 W m^{-2} at transition 2 (Fig. 5c and Table 1). A compensating increase of 8.4 W m^{-2} is contributed by the sensible heat flux at transition 1 (Fig. 5d and Table 1) because of the increased wind speeds but continued stable conditions in the lower atmosphere. However, at transition 2, the turbulent latent and sensible heat fluxes contribute 14.2 W m^{-2} to decrease F_{tot} due to the destabilized and drier lower atmosphere. Hence, the decrease of 58 W m^{-2} in F_{tot} from period 1 to period 3 is produced by the albedo effect (25.2 W m^{-2} or 43%), the change in Q_{si} (15.3 W m^{-2} or 26%), the change in Q_{li} (9.6 W m^{-2} or 17%), and the change in turbulent heat flux (6.1 W m^{-2} or 11%). The fact that the surface temperature changed very little minimized the compensating effect of decreases in Q_{lo}. Changes in C were negligible. Hence, all terms but C contributed 10% or more to the decrease in F_{tot}.

4. PACK ICE CHANGES

During July and August, the pack ice was about 2 m thick but melting rapidly as one might expect with a positive F_{tot} this entire time. Direct measurements of the melt rates and the partitioning of these rates between melting of the surface and bottom ice were made and are shown in Fig. 6. Surface melt rates of 1.8-2.3 cm/day occurred during period 1 before July 26 (JD207), while bottom melt rates were smaller near 0.5 cm/day. The loss of 2.3 - 2.5 cm of ice every day for an extended period caused concern for the longevity of the pack ice and the viability of the ice camp. During period 2, when the frontal passages of event E2 occurred, the surface melt decreased drastically to near 0.4 cm/day though the bottom melt increased to 1.2 cm/day. During period 3, both the bottom melt and the surface melt stayed essentially constant, and the SHEBA site was now losing about 1.5 cm of ice per day, with the majority being from bottom melt.

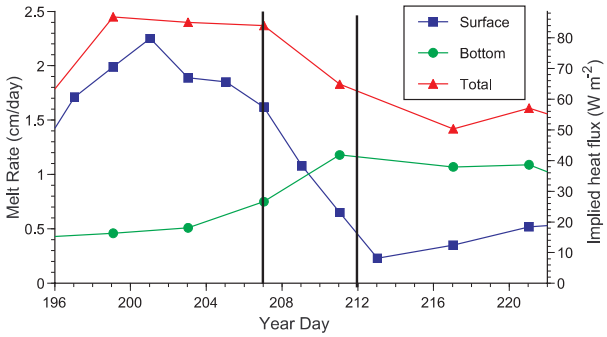

Fig. 6: Average pack ice surface and bottom melt rates calculated from approximately 80 thickness gauges. The surface melt rates use a 3-point running mean smoother. The gauges were located on a wide range of ice types including bare ice, ponded ice, and pressure ridges. The right-hand-side shows the heat flux corresponding to the observed melt rate, and the vertical black lines show the transitions from periods P1 to P2 and P2 to P3, respectively.

Further insight into the processes producing the changes in the ice pack mass balance can be obtained by noting that the measured melt rates correspond directly to a heat flux. The heat fluxes corresponding to the surface, bottom, and total melt rates are shown on the right side of Fig. 6 and are replotted on Fig. 4b to provide a comparison to the surface energy flux measurements. During period 1 and 2, the total heat flux required to provide the observed melt is equal to the observed heat flux going into the top of the ice. This implies that there is no oceanic heat flux to the bottom of the ice and that the little bottom melt that is occurring is due to heat flux through the ice from the top. As F_{tot} decreases in period 2, the surface melt decreases even more rapidly than the bottom melt increases. During period 3, the total flux from melting exceeds F_{tot}, implying that an oceanic heat flux contributes about 15 W m^{-2} to the melting at the bottom of the ice. Future examination of oceanographic data collected in the leads and under the pack ice should provide validation data for this hypothesis and further insights into the mechanisms for these transitions. Data may also be available to better understand the energy transfers and the melting processes within the virtually isothermal pack ice.

5. CONCLUSIONS

In this study, we have examined the impact of an atmospheric regime change, marked by several cold frontal passages, on the atmospheric environment, surface energy budget, and the pack ice melting. During the first part of this period before the regime change, a summertime surface energy regime dominated, with temperatures significantly above freezing only a few hundred meters above the surface, significant ice melt, and warming of the ocean surface in the leads. From July 26 - August 1 (JD 207-213), a major synoptic event drastically changed the environmental features and processes. Significant reductions occurred in the temperature throughout the troposphere (except near the surface), including the removal of above freezing temperatures (albeit only temporarily). All surface energy budget terms except conduction made significant contributions to the 64%decrease in the energy flux at the top of the ice. The largest contributor was due to the change in surface albedo (43%), followed by the decrease in incoming solar radiation (26%). Some terms, such as the incoming radiation and the atmospheric turbulent sensible heat flux, contributed differently at the two major transitions in the change of total heat flux associated with the first and last cold fronts of this regime transition.

This event also produced a significant reduction in the total ice melt rate and a change from predominantly surface melt to predominantly bottom melt. The surface energy flux appears to be the primary cause for both surface and bottom melt before the transition, while oceanic heat flux, possibly from energy previously stored in leads and mixed under the ice by the increased surface stress (Paulson and Pegau 2001), contributes significantly afterwards.

Clearly, this several-day atmospheric synoptic event made a major step towards the transition from summer to fall freeze-up. Further examination of cloud data and oceanographic data not used in this study is necessary to more completely understand the processes producing these changes.

6. ACKNOWLEDGEMENTS

We are indebted to the numerous individuals who supported the research activities at the SHEBA site, including the captains and crews of the Canadian icebreaker Des Grosseilliers. Discussions with Miles McPhee, Clayton Paulson, Scott Pegau, and Matthew Shupe helped identify this event as being significant for all parts of the SHEBA column. This research has been supported by NSF awards OPP-97-01766 to NOAA/ETL, OPP-0084322 to CIRES, OPP-97-02025 and OPP-00-84190 to CRREL, and OPP-97-01390 and OPP-00-84279 to NPS.

7. REFERENCES

Intrieri, J., C. W. Fairall, M. D. Shupe, P. O. G. Persson, E. L. Andreas, P. S. Guest, and R. E. Moritz, 2002: Annual cycle of Arctic surface cloud forcing at SHEBA. *J. Geophys. Res,* **107** (C10), 8039, doi:10.1029/2000JC000439.

Paulson, C. A., and W. S. Pegau, 2001: The summertime thermohaline evolution of an Arctic lead: Heat budget of the surface layer. *Preprints, Sixth Conf. on Polar Meteorology and Oceanography*, San Diego, CA, Amer. Meteor. Soc., 271-274.

Perovich, D., and 22 others, 1999: SHEBA: The surface heat budget of the Arctic Ocean. *EOS, Transactions, American Geophysical Union*, **80**, 481-486.

_____, T. C. Grenfell, B. Light, and P. V. Hobbs, 2002a: The seasonal evolution of Arctic sea ice albedo, *J. Geophys. Res.*, (10.1029/2000JC000438).

_____ ,J. A. Richter-Menge, W. B. Tucker III, 2002b: Seasonal changes in Arctic sea ice morphology. Annals of Glaciology, In press.

_____, W. B. Tucker III, and K. A. Ligett, 2002c: Aerial observations of the evolution of ice surface conditions during summer. (10.1029/2000JC000449)

Persson, P. Ola G., C. W. Fairall, E. L. Andreas, P. S. Guest, and D. K. Perovich, 2002: Measurements near the Atmospheric Surface Flux Group tower at SHEBA: Near-surface conditions and surface energy budget. *J. Geophys. Res.* **107**(C10), 8045, doi:10.1029/2000JC000705.

Ruffieux, D. R., P. Ola G. Persson, C. W. Fairall, and Dan E. Wolfe, 1995: Ice pack and lead surface energy budgets during LEADEX 92. *J. Geophys. Res.*, **100**, C3, 4593-4612.

Uttal, T., and 27 others, 2002: The surface heat budget of the Arctic, *Bull. Amer. Meteor. Soc.*, **83**, 255-275.